Myosin 6 Is Required for Iris Development and Normal Function of the Outer Retina

Ivy S. Samuels,[1,2] Brent A. Bell,[2] Gwen Sturgill-Short,[1,2] Lindsey A. Ebke,[2] Mary Rayborn,[2] Lanying Shi,[3] Patsy M. Nishina,[3] and Neal S. Peachey[1,2,4]

[1]Research Service, Louis Stokes Cleveland Veterans Affairs Medical Center, Cleveland, Ohio
[2]Department of Ophthalmic Research, Cole Eye Institute, Cleveland Clinic, Cleveland, Ohio
[3]The Jackson Laboratory, Bar Harbor, Maine
[4]Department of Ophthalmology, Cleveland Clinic Lerner College of Medicine at Case Western Reserve University, Cleveland, Ohio

PURPOSE. To determine the molecular basis and the pathologic consequences of a chemically induced mutation in the translational vision research models 89 (*tvrm89*) mouse model with ERG defects.

METHODS. Mice from a G3 *N*-ethyl-*N*-nitrosourea mutagenesis program were screened for behavioral abnormalities and defects in retinal function by ERGs. The chromosomal position for the recessive *tvrm89* mutation was determined in a genome-wide linkage analysis. The critical region was refined, and candidate genes were screened by direct sequencing. The *tvrm89* phenotype was characterized by circling behavior, in vivo ocular imaging, detailed ERG-based studies of the retina and RPE, and histological analysis of these structures.

RESULTS. The *tvrm89* mutation was localized to a region on chromosome 9 containing *Myo6*. Sequencing identified a T→C point mutation in the codon for amino acid 480 in *Myo6* that converts a leucine to a proline. This mutation does not confer a loss of protein expression levels; however, mice homozygous for the *Myo6tvrm89* mutation display an abnormal iris shape and attenuation of both strobe-flash ERGs and direct-current ERGs by 4 age weeks, neither of which is associated with photoreceptor loss.

CONCLUSIONS. The *tvrm89* phenotype mimics that reported for *Myosin6*-null mice, suggesting that the mutation confers a loss of myosin 6 protein function. The observation that homozygous *Myo6tvrm89* mice display reduced ERG a-wave and b-wave components, as well as components of the ERG attributed to RPE function, indicates that myosin 6 is necessary for the generation of proper responses of the outer retina to light.

Keywords: electroretinography, myosin, iris, retina

Myosins are actin-based motor proteins, coupling adenosine triphosphate (ATP) hydrolysis to mechanical motion along actin filaments. To date, more than 30 myosin proteins have been identified in species ranging from *Drosophila* to human, and they are known to contribute to essential cellular functions, including secretion, cell division, differentiation, and migration.[1] Myosin 6 is an unconventional myosin motor protein and is the only myosin that moves toward the minus end of the actin filament.[2]

In mice, only one functionally unique isoform of myosin 6 is expressed. The gene was first identified in the Snell's waltzer mouse (*sv*), which is characterized by circling behavior and head tossing secondary to vestibular dysfunction.[3,4] The presence of cochlear dysfunction in *Myo6sv* mice identified *Myo6* as a deafness gene.[4–6] *MYO6* mutations have subsequently been identified in autosomal recessive nonsyndromic deafness (DFNB37)[7,8] and autosomal dominant nonsyndromic hearing loss (DFNA22) in humans.[6,9,10] Myosin 6 has also been found in the retina and is highly expressed in photoreceptors and RPE cells[11–13] and throughout the inner retina. Notably, two of nine patients documented with DFNB37 displayed retinal abnormalities.[7] In photoreceptors, myosins are present in the actin-containing domain within the

connecting cilium of the inner segment, where the initiation and regulation of disc membrane morphogenesis occurs.[14] In the mouse photoreceptor, myosin 6 is localized exclusively to the inner segment. *Myo6sv* and two allelic mutants (*Myo6sv-2J* and *Myo6sv-4J*), which are all effective *Myo6*-null mutants, display reductions in a-wave and b-wave amplitudes as early as age 6 weeks,[15] with no evidence of photoreceptor degeneration or disruption in disc morphogenesis.[12] In the RPE, myosin 6 is localized to the periphery of the cell and colocalizes with LysoTracker[12] corroborating its role in vesicle trafficking[16–19] and providing a potential explanation for the functional abnormalities found despite the absence of anatomical changes to the retina.

A large number of new mouse models that demonstrate irregular structural and/or functional eye phenotypes have been developed in a mutagenesis program conducted at The Jackson Laboratory.[20] The translational vision research models (TVRM) program uses *N*-ethyl-*N*-nitrosourea (ENU) to induce random mutations, and neurological and ocular screens are used to identify mutants of interest. As described herein, the *tvrm89* mutant was identified by its circling behavior, and the mutation involved was subsequently identified as a leucine to proline substitution in myosin 6.

Myo6^tvrm89 mutants phenocopy, in many respects, the sensory abnormalities identified in *Myo6^sv*, *Myo6^sv-2J*, and *Myo6^sv-4J* mice. Unlike these well-studied mutants, myosin 6 protein expression is retained in the *Myo6^tvrm89*-mutant retina. The *Myo6^tvrm89* mouse provides a novel mutant for *Myo6* that confers a loss of function but does not affect expression of the protein.

METHODS

Mice: Mutagenesis, Mapping, and Genotyping

All animal procedures were approved by the institutional animal care and use committees of the institutions involved and are in agreement with the ARVO Statement for the Use of Animals in Ophthalmic and Vision Research. Homozygous *tvrm89* mice were identified from a mutagenesis program[20] in which male C57BL/6J (B6) mice were mutagenized with ENU administered in intraperitoneal injections of 80 mg/kg for 3 weeks.[21] The G3 offspring, generated using a three-generation backcross mating scheme to identify recessive mutations,[22] were screened by a series of neurological protocols. The *tvrm89* mutant was identified based on its circling behavior and head bobbing, indicative of inner ear dysfunction.

To map the gene involved, which is inherited as an autosomal recessive trait, B6 *tvrm89* homozygous female mice were mated to male DBA/2J mice to generate F1 progeny, which were subsequently intercrossed. The F2 progeny were assessed at age 12 weeks, and DNA was isolated from tail snips using a modified version of published methods.[23] A genome-wide scan to determine the chromosomal location of *tvrm89* was performed with simple sequence-length polymorphic markers. Products of PCR were separated by electrophoresis on a 4% agarose gel (MetaPhor; FMC, Rockland, ME), stained with ethidium bromide, and visualized by UV light.

For sequencing of candidate genes, RNA and cDNA were prepared from three mutant mice and three control B6 mice. The RNA was isolated from snap-frozen eyes (TRIzol; Invitrogen, Carlsbad, CA) according to the manufacturer's instructions. The cDNA was generated with a reverse transcription kit (Retroscript; Ambion, Austin, TX). The *Myo6* coding region was amplified from cDNA using PCR amplification, and purified products were sequenced.

The *tvrm89* mouse colony at The Jackson Laboratory is maintained by heterozygous matings. Mice were shipped to the Cleveland Clinic to establish a satellite colony that is maintained on a 14-hour light–10-hour dark cycle.

An allele-specific PCR assay for *Myo6^tvrm89* was established, and PCR amplification of the region was carried out as follows: (1) 94°C for 2 minutes, (2) 94°C for 20 seconds, (3) annealing temperature of 60°C for 10 seconds, and (4) 65°C for 50 seconds; steps two through four were repeated for 40 cycles, followed by one cycle at 65°C for 7 minutes. The following oligonucleotides were used for PCR amplification:

F1: 5′-AGCCCAGACTATTAACGTACATT-3′
R1: 5′-CCTTTCATTAAAAAACTGTTGTG-3′
R2: 5′-CCTTCAGGATGGTTTCATTAAAAAACTGTAGGA-3′

Scanning Laser Ophthalmoscopy and Spectral-Domain Optical Coherence Tomography

Mice were anesthetized with 64 mg/kg of sodium pentobarbital. Mydriasis was induced by administration of 1 μL of 0.5% Mydrin-P (tropicamide-phenylephrine combination) drops (Santen Pharmaceutical Co., Ltd., Osaka, Japan). The drops were gently massaged into the eye by artificially blinking the eyelids. Eyes were then immediately covered with Systane Ultra artificial tears (Alcon Laboratories, Inc., Ft. Worth, TX). Mice were then placed in a warmed, humidified, oxygenated acrylic plastic sheet chamber for a minimum of 5 minutes to permit time for pupil dilation. Mice were then removed for imaging by scanning laser ophthalmoscopy (SLO) (model HRA2; Heidelberg Engineering, Inc., Vista, CA) and spectral-domain optical coherence tomography (SDOCT) (model Envisu SDOIS; Bioptigen, Inc., Research Triangle Park, NC). The SLO imaging involved collection of different imaging modalities, including dark-field reflectance and autofluorescent images with both blue (488 nm) and infrared (795 nm and 830 nm) illumination wavelengths. Using a wide-field objective lens with a 55° field of view (FOV), retinal images were collected with the optic nerve centrally positioned. Additional views of the peripheral regions were obtained to further investigate the nasal, temporal, superior, and inferior quadrants. Eyes were occasionally rehydrated with balanced salt solution or Systane Ultra artificial ears (Alcon Laboratories) and mechanically massaged to simulate blinking as needed. After SLO imaging, the mouse was transferred to the Envisu SDOIS system (Bioptigen, Inc.) for SDOCT imaging. The SDOCT volumetric scans (250 a-scans per b-scan × 250 b-scans per volume) were obtained with the optic nerve centrally located within the FOV. Using a 50° objective lens, the SDOIS system afforded a retinal FOV of approximately 1.5 mm, with an axial, in-depth resolution of approximately 6 μm. After imaging, both eyes received bacitracin zinc and polymyxin B sulfate ophthalmic ointment (Bausch & Lomb, Inc., Tampa, FL) to prevent corneal dehydration. During recovery, mice were placed in a bottom-warmed (33–36°C), oxygenated (21%–60%) acrylic plastic sheet chamber until they fully recovered from general anesthesia.

Electroretinography

After overnight dark adaptation, mice were anesthetized (80 mg/kg of ketamine and 16 mg/kg of xylazine), the cornea was anesthetized (1% proparacaine hydrochloride), and the pupils were dilated (1% tropicamide, 2.5% phenylephrine hydrochloride, and 1% cyclopentolate). Mice were placed on a temperature-regulated heating pad throughout each recording session.

The protocols used to record ERG components generated by the outer neural retina or the RPE have been described.[24] In brief, responses of the outer retina were recorded with a stainless steel electrode referenced to a needle electrode placed in the cheek in response to strobe-flash stimuli presented in the dark or superimposed on a steady 20 candela (cd)/m^2 rod-desensitizing adapting field. The amplitude of the a-wave was measured 8 milliseconds after flash onset from the prestimulus baseline. The amplitude of the b-wave was measured from the a-wave to the peak of the b-wave or, if no a-wave was present, from the prestimulus baseline. Implicit times were measured from the time of flash onset to the a-wave trough or the b-wave peak.

Components of the direct-current coupled (dc)–ERG generated by the RPE were recorded with a silver/silver chloride electrode bridged to the corneal surface with Hanks' balanced salt solution in response to stimuli presented for 7 minutes. The amplitude of the c-wave was measured from the prestimulus baseline to the peak of the c-wave. The amplitude of the fast oscillation (FO) was measured from the c-wave peak to the trough of the FO. The amplitude of the light peak (LP)
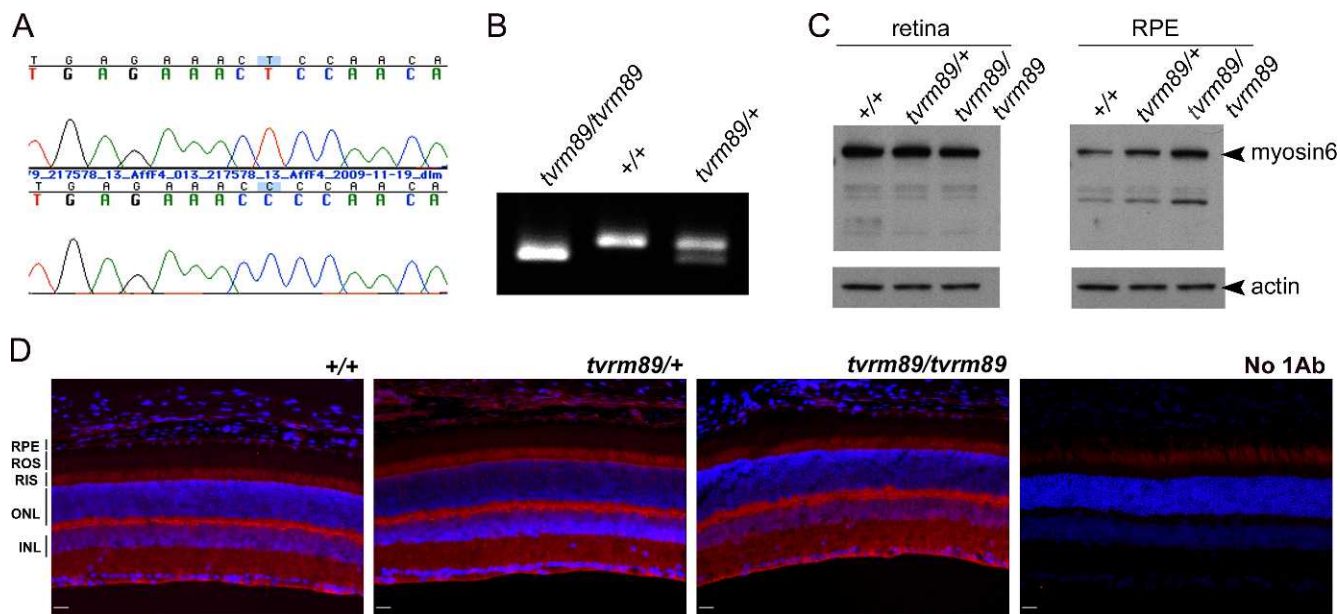
FIGURE 1. The *tvrm89* mutants bear a point mutation in *Myosin6* but retain myosin 6 protein levels. (**A**) Positional cloning and direct sequencing demonstrate a T→C transition mutation found in homozygous *tvrm89* mutants. (**B**) Allele-specific genotyping was accomplished using PCR amplification of DNA extracted from tail snips. (**C**) Western blot analysis of retinal (*left*) and RPE (*right*) protein lysates demonstrates myosin 6 protein levels in wild-type (+/+), heterozygous (*tvrm89/+*), and homozygous (*tvrm89/tvrm89*) mice. Actin serves as a loading control. (**D**) Cryosections of eyecups from +/+, *tvrm89/+*, and *tvrm89/tvrm89* mice were immunostained with Myosin-VI antibody (*red*) and counterstained with 4′,6-diamidino-2-phenylindole (*blue*). Myosin 6 is present in all three genotypes and is highest in rod inner segments and the inner retina. At the *right* is the no primary antibody control. Low levels of autofluorescence are found in the rod outer segments; however, no specific immunostaining was apparent. *Scale bar*: 20 μm.

was measured from the FO trough to the asymptotic value. The amplitude of the off-response was measured from the LP asymptote to the peak of the off-response.

Histology and Immunohistochemistry

After mice were killed, the superior cornea was marked before enucleation. After removal of the cornea and lens, eyes were fixed in 0.1 M sodium phosphate buffer (pH 7.4) containing 4% paraformaldehyde for 4 hours. The posterior pole was then immersed through a graded series of sucrose solutions as follows: 10% for 1 hour, 20% for 1 hour, and 30% overnight. Eyes were embedded in optimum temperature cutting compound freezing medium, flash frozen on dry ice, and immediately transferred to −80°C. Tissue was sectioned at 10-
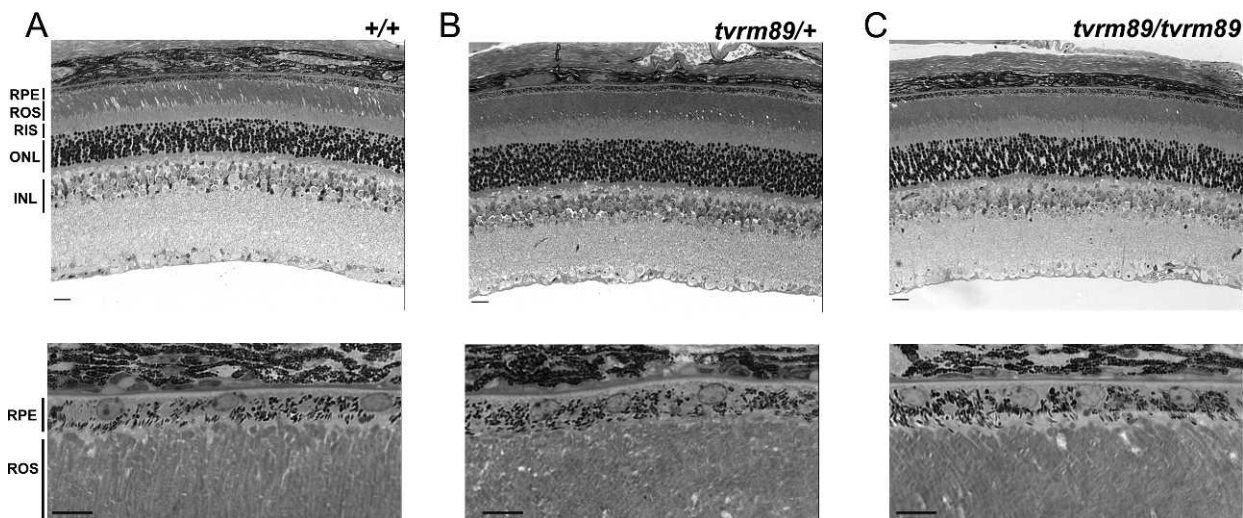

FIGURE 2. Normal retinal anatomy in *Myo6^tvrm89* mutants. Retinal cross sections obtained from control *Myo6^+/+* (**A**), *Myo6^tvrm89/+* (**B**), and mutant *Myo6^tvrm89/tvrm89* (**C**) mice. Retinal histology was normal in all genotypes. *Top*: Representative light micrographs of the retina from ultrathin sections of adult eyecups. *Scale bar*: 20 μm. *Bottom*: Representative light micrographs displaying RPE morphology from semithin sections of adult eyecups. *Scale bar*: 10 μm. INL, inner nuclear layer; ONL, outer nuclear layer; RIS, rod inner segment; ROS, rod outer segment.
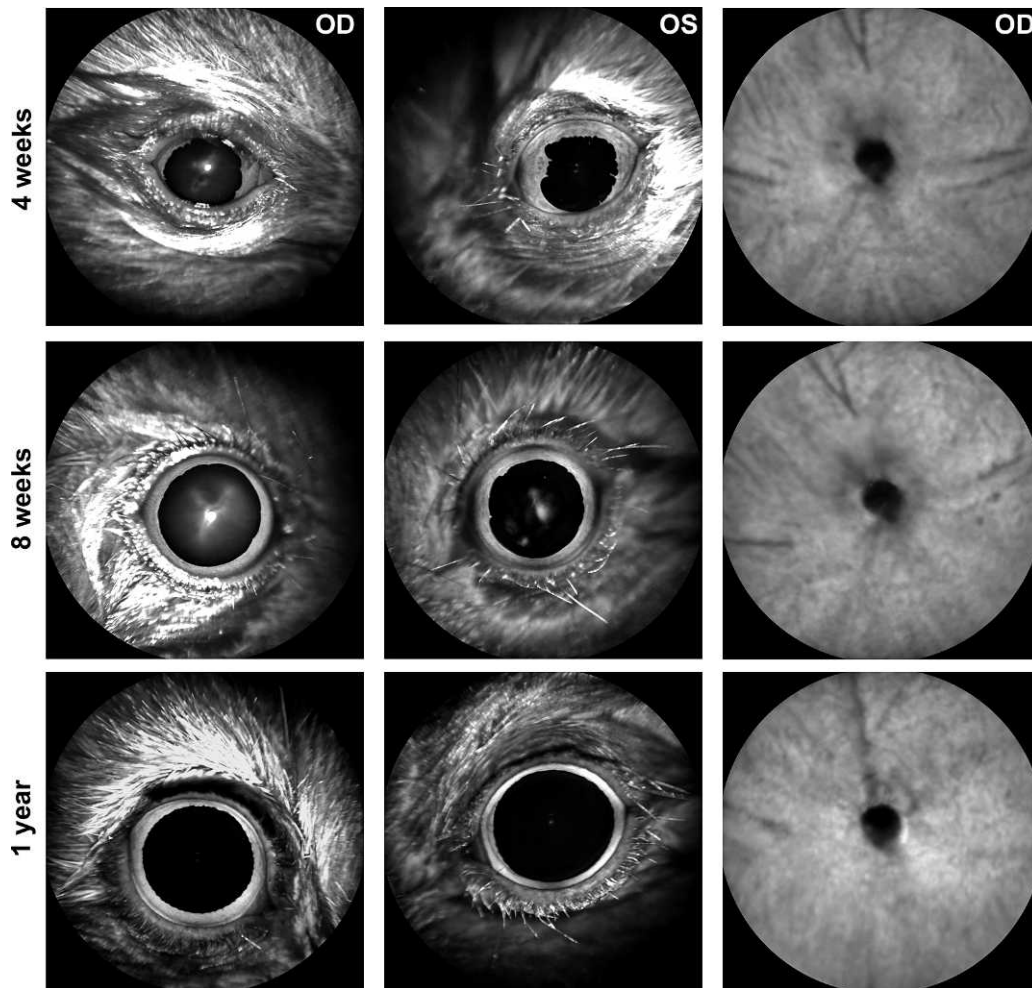
FIGURE 3. Iris but not fundus abnormalities in homozygous *Myo6^{tvrm89}* mice. *Myo6^{tvrm89}* mutants display iris abnormalities (synechiae) that resolve with age. *Left, middle*: Low-magnification photomicrographs obtained by SLO displaying scalloped pupil shape in both left and right eyes at 4 weeks (*top*), 8 weeks (*middle*), and 1 year or older (*bottom*). *Right*: Infrared (dark field) SLO images of the retina taken at 4 weeks (*top*), 8 weeks (*middle*), and 1 year (*bottom*). No abnormalities were observed in the retina or the RPE at any age.

μm thickness with a cryostat (Leica, Wetzlar, Germany) at −30°C, mounted on Superfrost slides (Fisherbrand, Pittsburgh, PA), and stored at −80°C until processed. Sections were incubated in 0.1% Triton X-100 and 10% normal goat serum in PBS for 1 hour (PBS-T) at room temperature and then washed three times with PBS for 5 minutes each. The sections were incubated overnight at 4°C with the primary antibody. Sections were rinsed with PBS-T three times for 10 minutes each and incubated with secondary antibody (AlexaFluor 594, 1:500; Molecular Probes, Eugene, OR) for 1 hour at RT. After rinsing sections three times for 5 minutes each with PBS-T, sections were mounted with 4′,6-diamidino-2-phenylindole (Vectashield; Vector Laboratories, Burlingame, CA) and coverslipped. Primary antibody was rabbit anti–Myosin-VI (1:200; Proteus BioSciences, Inc., Ramona, CA).

For light microscopy, eyes were fixed in 0.1 M sodium cacodylate buffer (pH 7.4) containing 2% formaldehyde and 2.5% glutaraldehyde. The tissues were then osmicated, dehydrated though a graded ethanol series, and embedded in epoxy resin (Epon/Araldite; Polysciences, Inc., Washington, PA). Semithin sections (1 μm) were cut approximately along the horizontal meridian and through the optic nerve and stained with toluidine blue O for evaluation.

Western Blot

Retinal and RPE tissues were dissected from enucleated eyes and frozen in lysis buffer (50 mM Tris [pH 8.0], 150 mM sodium chloride, 10% glycerol, 0.5% Triton X-100, and 0.1% NP40) supplemented with protease inhibitors (Roche Applied Science, Indianapolis, IN). Lysates were homogenized by manual grinding with a disposable pestle within a microcentrifuge tube three times, followed by five brief sonication pulses. Lysates were digested at 4°C for 1 hour, followed by centrifugation at 6600g for 10 minutes at 4°C. The supernatants were collected, and the total protein in each sample was determined by bicinchronic acid assay (Thermo Scientific, Rockford, IL) according to the manufacturer's instructions. Samples containing 25 μg of total protein for retina or 10 μg of protein for RPE with Lane Marker Reducing Sample Buffer (Thermo Scientific) were heated to 95°C for 5 minutes to denature the samples. Proteins were separated on 4% to 20% Tris-glycine SDS-PAGE gels and transferred to polyvinylidene difluoride membranes using 1× running buffer and transfer buffer (Bio-Rad Laboratories, Hercules, CA). Membranes were blocked for 1 hour in a 5% milk solution in Tris-buffered saline containing 0.1% Tween-20 (TBS-T). The primary antibodies were applied in blocking solution overnight at 4°C. After washes with TBS-T, the
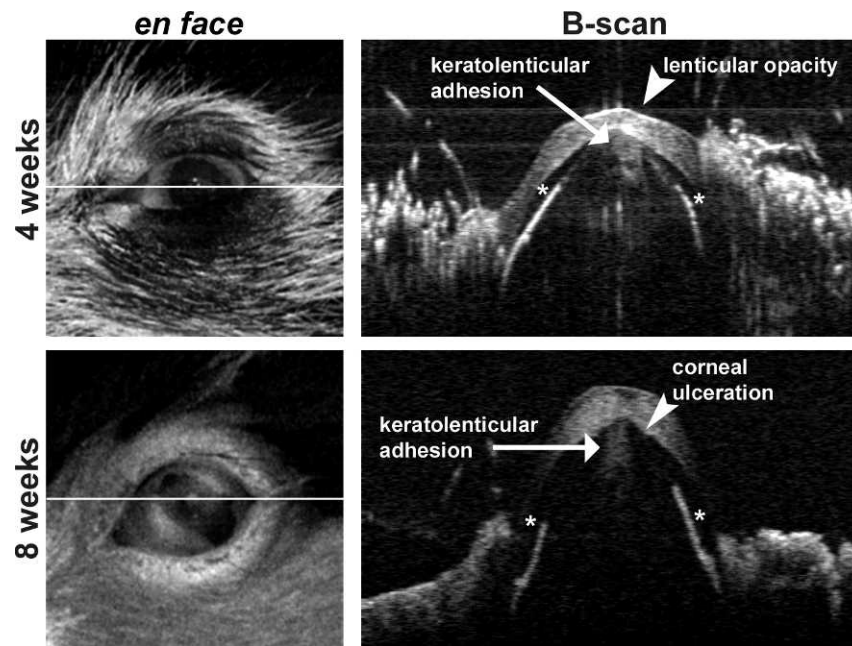
FIGURE 4. Abnormal iris shape and anterior segment morphology in homozygous $Myo6^{tvrm89}$ mice. The SDOCT imaging of homozygous $Myo6^{tvrm89}$ mice found with bilateral synechiae revealed abnormal anterior segment morphology in approximately 50% (4/7) of animals. The *horizontal line* through the en face fundus image (*left*) indicates the location of a single SDOCT B-scan frame (*right*). *Asterisks* denote anterior chamber. *Arrowhead* at the *top* marks the lenticular opacity. *Arrowhead* at the *bottom* marks the corneal ulceration. *Arrows* indicate keratolenticular adhesions.

peroxidase-conjugated secondary antibodies (Jackson Immuno-Research Laboratories, Inc., West Grove, PA) were applied at 1:5000 in blocking buffer for 1 hour at room temperature, and proteins were detected by enhanced chemiluminescence (Western Lightning kit; Perkin-Elmer, Waltham, MA). Primary antibodies used were Myosin VI (1:200; Proteus BioSciences, Inc.) and β-actin (1:1000; Abcam, Cambridge, MA).

RESULTS

A *Myo6* Missense Mutation Confers Pathology in *tvrm89* Homozygous Mice

Linkage analysis localized the gene mutated in *tvrm89* mice to a region of chromosome 9 containing *Myo6*. Because the phenotype of affected *tvrm89* homozygotes matched that of $Myo6^{sv/sv}$ mice,[3] including elevated auditory brainstem response threshold (data not shown), the coding region of *Myo6* was sequenced. We detected a T→C nucleotide transition that converts a leucine (CTC) to a proline (CCC) at amino acid 480 (Fig. 1A). The first 759 amino acids of mouse myosin 6 represent the head-motor region of the protein containing both the ATP-binding domain and the actin-binding sites (http://www.uniprot.org/uniprot/Q9UM54 [in the public domain]). Conversion of amino acid 480 from leucine to proline is likely to affect actin and/or ATP binding and to destabilize protein structure because of the substitution of proline's unique 5-membered ring into the main-chain conformation.

The PCR analysis of cDNA encompassing the *tvrm89* mutation confirmed the change in both the F2 intercross and *tvrm89* maintenance colony and was used for genotyping *Myo6* mutants because the products demonstrate a size difference (wild type is 135 base pair [bp] and mutant is 108 bp) (Fig. 1B). From this point forward, the *tvrm89* allele will be referred to as $Myo6^{tvrm89}$.

Western blot analyses of lysates generated from retina or RPE were probed with an antibody that recognizes an epitope containing amino acids 1049 through 1254 within the tail region of myosin 6. The immunoblot (Fig. 1C) demonstrated that myosin 6 is retained in homozygous $Myo6^{tvrm89}$ mutants. Localization of myosin 6 was investigated by fluorescent immunohistochemistry on frozen cryosections from adult mice. No differences in myosin 6 expression or localization were apparent between homozygous $Myo6^{tvrm89}$ mutants and control littermates (Fig. 1D). General histological analysis of mutant mice was further performed using semithin epoxy resin sections of adult eyecups, and no overt changes were identified in any retinal layer (Fig. 2, top). High-magnification micrographs of the RPE–outer segment interface demonstrated normal morphology (Fig. 2, bottom).

Iris Abnormalities in Homozygous $Myo6^{tvrm89}$ Mice

At age 4 weeks, in vivo imaging demonstrated a bilateral, abnormal, scalloped pupil shape in homozygous $Myo6^{tvrm89}$ mutants (Fig. 3, left, middle). This phenotype was fully penetrant and generally caused by formation of synechiae, including adhesions of the iris to the cornea (anterior synechiae) or to the lens (posterior synechiae). Subsequent imaging at 8 weeks and at 1 year or older showed similar but less pronounced findings (Fig. 3). The SDOCT imaging of mutants with bilateral synechiae revealed multiple abnormalities within the anterior segment at both 4 weeks and 8 weeks (Fig. 4). At 4 weeks, a lenticular opacity (arrowhead) can be observed immediately adjacent to a keratolenticular adhesion (arrow) involving the posterior cornea and the lens. At 8 weeks, the misshapen iris and keratolenticular adhesion persist, but the lenticular opacity is less apparent and somewhat resolved. A corneal ulceration (arrowhead) can also be observed on the posterior cornea at 8 weeks. Anterior chamber cavities are also abnormally small at both time points (asterisks). The SLO of
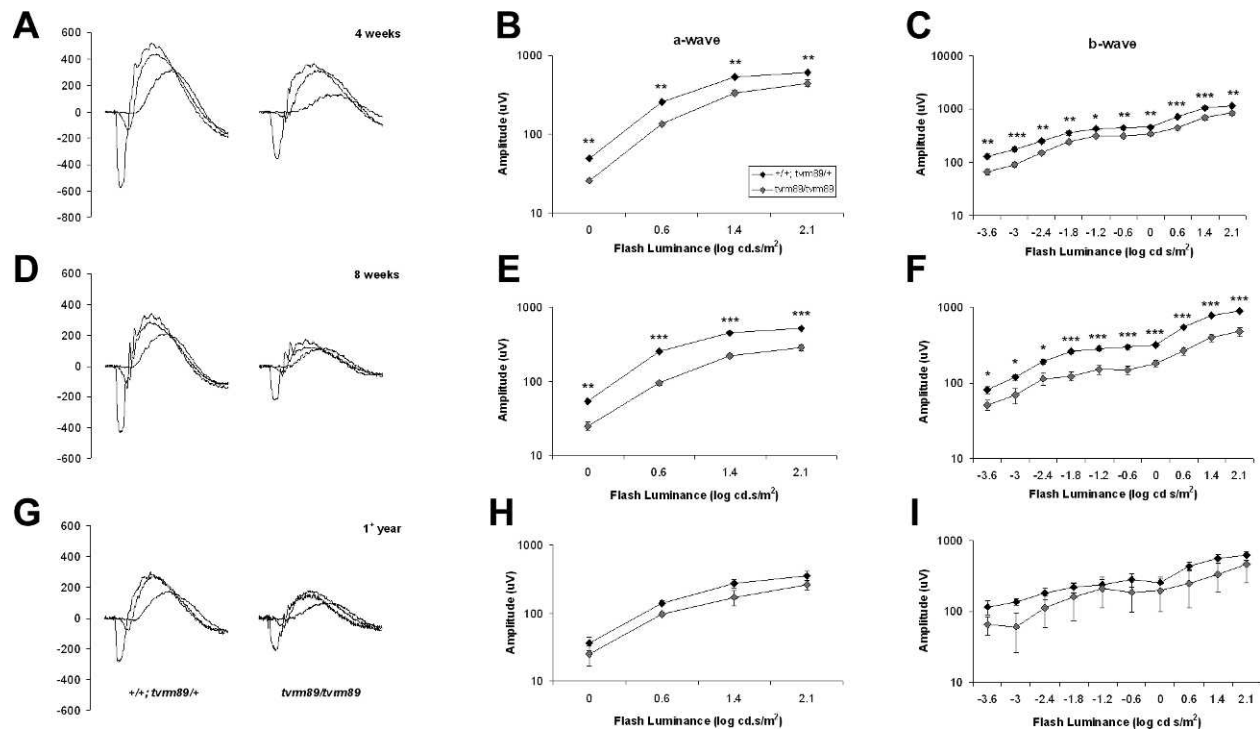
FIGURE 5. Homozygous *Myo6^tvrm89* mice display attenuated ERGs. Averaged strobe-flash ERG responses at 4 weeks (**A–C**), 8 weeks (**D–F**), and 1 year or older (**G–I**). (**A, D, G**) Averaged tracings from control (+/+ and *tvrm89*/+) and mutant (*tvrm89/tvrm89*) mice in response to stimuli of −2.4, −0.6, and 2.4 log cd s/m². (**B, E, H**) The a-wave luminance-response functions (*points* indicate the average ± SEM). (**C, F, I**) The b-wave luminance-response functions (*points* indicate the average ± SEM). Data summarize results from 22 control and 10 mutants at 4 weeks, from 24 controls and 7 mutants at 8 weeks, and from 4 controls and 2 mutants at 1 year or older. ***P ≤ 0.0001, **P ≤ 0.001, *P ≤ 0.01 by Student's *t*-test.

mice at 4 weeks, 8 weeks, or 1 year or older did not identify any clinical RPE or retinal abnormalities (Fig. 3, right).

Homozygous *Myo6^tvrm89* Mutants Display Reduced Light-Evoked Responses of the Retina and RPE

The ERG is reduced in amplitude in *Myo6^sv/sv* mice.[12] To determine whether this feature is shared in the *Myo6^tvrm89* mutants (Fig. 1C), we used ERGs to examine the function of the outer retina and of the RPE. The strobe-flash ERG depicts both photoreceptor activity in the form of the a-wave and bipolar cell function as revealed by the b-wave. Figure 5 shows averaged ERG tracings at 4 weeks (A), 8 weeks (D), and 1 year or older (G) in response to a subset of the strobe-flash stimuli (−2.4, −0.6, and 1.4 log cd s/m², respectively). At each age, the overall amplitude of ERGs obtained from homozygous *Myo6^tvrm89* mutants was reduced compared with that of control (+/+ and *tvrm89*/+) littermates. Luminance-response functions for the major components of the ERG are shown in Figure 5 at 4 weeks (B, C), 8 weeks (E, F), and 1 year or older (H, I). Compared with control, response functions of homozygous *Myo6^tvrm89* mutants are reduced by a consistent factor across flash luminance. The amplitude of the a-wave was reduced on average by 40% at 4 weeks (B), 53% at 8 weeks (E), and 31% at 1 year or older (H), and the amplitude of the b-wave was reduced by 35% at 4 weeks (C), 46% at 8 weeks (F), and 34% at 1 year or older (I). These reductions are comparable to the 25% (a-wave) and 30% (b-wave) reductions reported in *Myo6^sv/sv* mutants aged 6 to 7 weeks.[12] We found no change in b-wave latency at any age (data not shown).

We next assessed the light-evoked responses of the RPE. Figure 6A shows representative dc-ERG tracings from homozygous mutant *Myo6^tvrm89* and control mice at 4 weeks and 8

weeks. The four main components of the dc-ERG (Fig. 6A) are generated because of changes in ion conductance across the basal and apical RPE membranes in response to light stimuli.[24] Compared with control, the overall amplitude of the dc-ERG was reduced in homozygous *Myo6^tvrm89* mutants at both age 4 weeks and 8 weeks; as shown in Figure 6, the individual components at these two ages were reduced by 36% and 30% (respectively) for the c-wave (B), 45% and 27% for the FO (C), and 31% and 25% for the LP (D), as well as by 18% at both ages for the off-response (E). Collectively, these results demonstrate that ERG components generated by the RPE response were diminished in homozygous *Myo6^tvrm89* mutants but that the magnitude of this reduction was less pronounced at age 8 weeks.

RPE Function in Homozygous *Myo6^tvrm89* Mice Is Reduced but Is Spared Relative to Photoreceptor Activity

The dc-ERG is generated secondary to rod photoreceptor activity.[24,25] As a consequence, a reduced dc-ERG could reflect RPE dysfunction or a reduced effective stimulus from rod photoreceptors. In view of the reduced a-wave of homozygous *Myo6^tvrm89* mutants (Fig. 5), we examined the relation between rod photoreceptor activity and the individual dc-ERG components of homozygous *Myo6^tvrm89*-mutant mice. Each panel of Figure 7 shows the amplitude of a dc-ERG component (c-wave [A], FO [B], LP [C], and off-response [D]) plotted against the amplitude of the a-wave elicited by a high-luminance stimulus after each response measure was normalized to the control average. When the dc-ERG is reduced beyond the a-wave, the plotted points fall below the diagonal line; points fall along the diagonal line when the response
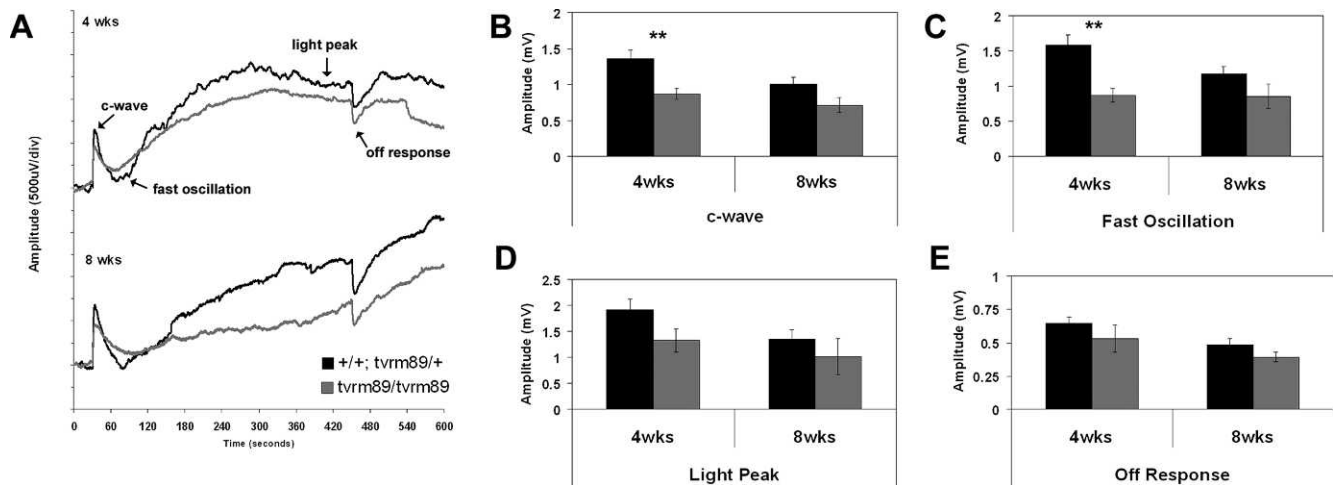
FIGURE 6. The RPE function is reduced in homozygous *Myo6^tvrm89* mice. (**A**) Representative dc-ERGs of control (+/+ or *tvrm89*/+) mice (*black*) and mutant (*tvrm89*/*tvrm89*) mice (*gray*) at 4 weeks and 8 weeks. Baseline measurements are recorded for 30 seconds before initiation of a 7-minute light stimulus of 2.4 log cd/m². The major dc-ERG components are labeled. (**B–E**) Amplitude of c-wave (**B**), FO (**C**), LP (**D**), and off-response (**E**) obtained from mice aged 4 weeks or 8 weeks. *Bars* indicate the average ± SEM of 20 control and 7 mutant mice at 4 weeks and of 15 control and 7 mutant mice at 8 weeks. **$P \leq 0.001$ by Student's *t*-test.

measures are reduced by equal amounts. In general, at 4 weeks points fall close to the diagonal, indicating that dc-ERG and ERG a-waves are reduced by equivalent amounts. At 8 weeks, points fall above the diagonal, demonstrating that RPE function is spared despite the decrease in photoreceptor activity.

Reduced Cone ERGs in Homozygous *Myo6^tvrm89* Mice

Myosin 6 localization has been reported in cone ellipsoids of various fish species,[11,13] and it is highly expressed at the outer limiting membrane and inner segment of mouse photorecep-
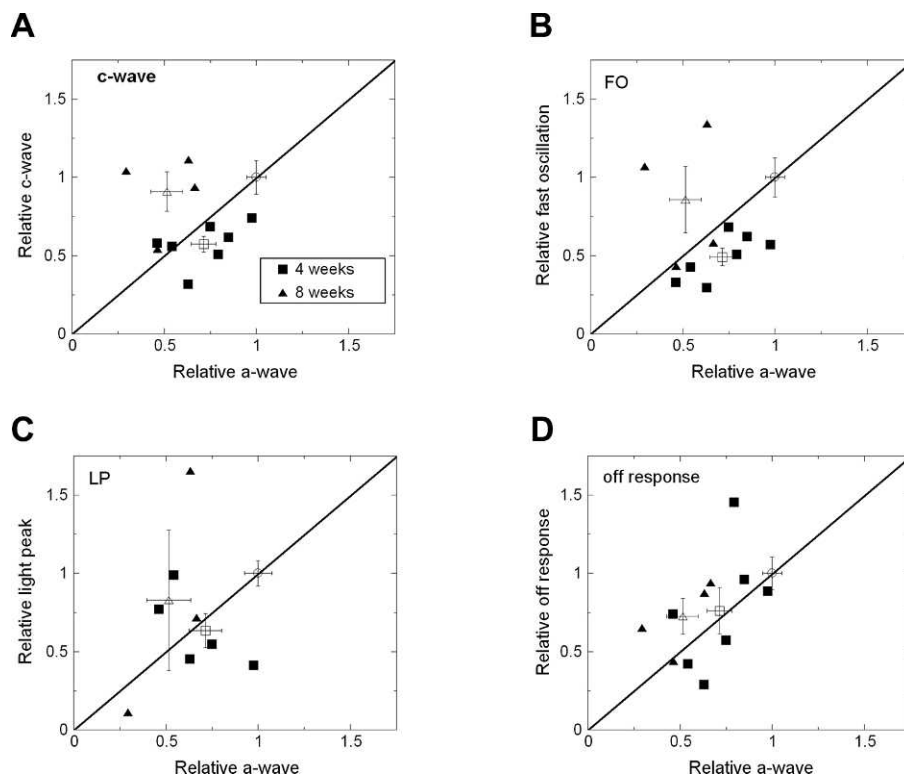

FIGURE 7. The RPE function is equivalent to or better than photoreceptor activity in homozygous *Myo6^tvrm89* mice. Relative changes in amplitude of each major dc-ERG component (c-wave [**A**], FO [**B**], LP [**C**], and off-response [**D**]) as a function of a-wave amplitude in response to a light stimulus of 1.4 log cd s/m². Each *filled point* indicates data obtained from an individual homozygous *Myo6^tvrm89*-mutant mouse plotted relative to the average control response. Data sets from 4 weeks are denoted by *squares*, and data sets from 8 weeks are denoted by *triangles*. The average ± SEM for each age is represented by an *open square* (4 weeks) or *open triangle* (8 weeks). The average ± SEM for control mice is represented by an *open circle*. The *diagonal line* indicates an equivalent reduction in the a-wave and each major component of the dc-ERG.
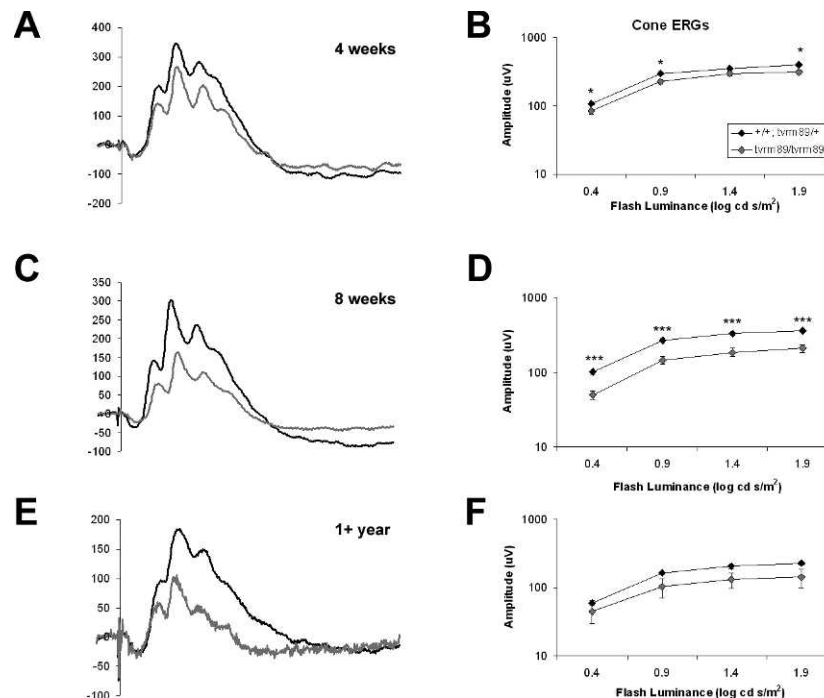
FIGURE 8. Cone ERG is reduced in homozygous $Myo6^{tvrm89}$ mice. Averaged light-adapted strobe-flash ERG responses at 4 weeks (A, B), 8 weeks (C, D), and 1 year or older (E, F). Mice were light adapted for 7 minutes following dark-adapted testing and underwent strobe-flash ERGs under a steady rod-desensitizing adapting field (20 cd/m^2). (A, C, E) Representative tracings from control (+/+ and tvrm89/+) and mutant (tvrm89/tvrm89) mice in response to a light stimulus of 1.9 log cd s/m^2. (B, D, F) Cone ERG amplitude measured from the peak of the b-wave to the amplitude of the a-wave at 8 milliseconds. *Data points* indicate the average ± SEM of 22 control and 10 homozygous $Myo6^{tvrm89}$ mice at age 4 weeks, of 24 control and 7 homozygous $Myo6^{tvrm89}$ mice at age 8 weeks, and of 4 control and 2 homozygous $Myo6^{tvrm89}$ mice at age 1 year or older. ***$P \le 0.0001$, **$P \le 0.001$, *$P \le 0.01$ by Student's t-test.

tors[12] (Fig. 1). Therefore, we assessed the cone ERGs of homozygous $Myo6^{tvrm89}$ mice. Figure 8 shows representative responses of homozygous mutant $Myo6^{tvrm89}$ and control mice elicited by a 1.9 log cd s/m^2 flash stimulus for mice aged 4 weeks (A), 8 weeks (C), or 1 year or older (E). As shown in Figure 8, the cone ERG is reduced by a comparable degree across flash luminance, averaging 21% at 4 weeks (B), 38% at 8 weeks (D), and 34% at 1 year or older (F).

DISCUSSION

Myosin 6 is involved in many cellular processes important to sensory function.[26,27] Herein, we describe the retinal phenotype of the $Myo6^{tvrm89}$ mutant that carries a novel missense mutation in the motor domain of $Myosin6$. Our results add to the literature noting critical roles for myosin 6 at the inner and outer ear stereocilia in mice and in human deafness.[4,15,28–33] Moreover, our analysis of the functional and structural effects of the $tvrm89$ mutation provides a detailed report of the retinal phenotype in $Myo6$ mutants.

Unlike previously described $Myo6$ mutants, which involve null mutations that result in a loss of myosin 6 in the actin-rich domains within the retina/RPE, including rod photoreceptor inner segments, horizontal cells, and Müller glia,[11,13,34] myosin 6 protein expression is retained in the homozygous $Myo6^{tvrm89}$ retina (Fig. 2). This feature indicates that the $Myo6^{tvrm89}$ mouse model presented herein may provide insight into phenotypic features attributed to loss of myosin 6 function.

Iris Abnormalities in $Myo6^{tvrm89}$-Mutant Mice

A novel finding in the homozygous $Myo6^{tvrm89}$ mutant is the scalloped shape of the iris margin and abnormal morphology of

the anterior segment (Figs. 3, 4). A similar feature was not reported for any of the $Myo6^{sv}$ strains; however, it is unknown if this was because the iris abnormalities were not present or were missed. Bilateral synechiae were present in all homozygous $Myo6^{tvrm89}$ mutants, and approximately 50% of these animals also displayed lesions within the anterior chamber (Figs. 3, 4). We noted that these phenotypic features typically became less pronounced with age in the majority of animals imaged, which may be attributable to the use of mydriatics for ERG studies. The mydriatics and/or cyclopegics utilized for routine ERG studies are known to break synechiae and are used clinically in the treatment of iritis and iridocyclitis.[35] Consistent with this idea, posterior and anterior adhesions were visualized at 4 weeks and were maintained at the 8-week time point in the subset of animals that only underwent anesthesia by isofluorane inhalation and which were never treated with xylazine or topical mydriatics (Fig. 4).

Nonprogressive Reduction in Retinal Function of $Myo6^{tvrm89}$ Mice Without an Anatomical Correlate

Our detailed ERG analysis demonstrated that retinal function was reduced in 4-week-old homozygous $Myo6^{tvrm89}$ mutants, the earliest age examined. The $Myo6^{tvrm89}$-mutant phenotype, which involves reduced ERG amplitude in the face of normal retinal structure, is unusual but has been reported in other models and could reflect a reduced photoreceptor dark current, altered regulation of ions and pH in the subretinal space, a change in resistance of the retinal circuit through which the ERG is recorded, or some other mechanism.[36–38]

The dark current is the steady influx of a primarily sodium ion current that occurs in photoreceptors in the dark, maintaining them in a depolarized state. Upon presentation

of light stimuli, the cation channels close, and photoreceptors hyperpolarize, releasing neurotransmitters to second-order neurons. Changes in the distribution or expression of the sodium ion channels or sodium-calcium exchanger in the rod outer segment could thus lead to reductions in both photoreceptor activity and responses of RPE and bipolar cells.

The general decrease in retinal function that we observed in homozygous $Myo6^{tvrm89}$ mutants could alternatively relate to a change in ion conductance across the RPE and/or a change in pH homeostasis that can occur in response to altered function of the endolysosomal pathway. Myosin 6 is associated with both the autophagosome[39] and lysosome,[16–19] where the mutant form of myosin 6 could prevent either proper phagocytosis of shed outer segments, exchange of visual cycle components, or disk turnover and morphogenesis. Notably, we found that myosin 6 localization is unchanged in homozygous $Myo6^{tvrm89}$ mice (Fig. 1D) but that its protein expression is higher within the RPE compared with wild-type and heterozygous mice (Fig. 1C). Within polarized epithelial cells such as the RPE, myosin 6 internalizes and transports receptors away from apical microvilli via clathrin-mediated endocytosis.[2,11,12,17,26,31,40–46] Myosin 6 is known to mediate endocytosis of the cystic fibrosis transmembrane receptor (CFTR) in polarized epithelial cells.[47,48] Cystic fibrosis transmembrane receptor underlies a chloride ion conductance that is partially responsible for generation of the FO. In $Myosin6$-null mice, CFTR expression is maintained on the apical membrane of intestinal epithelium.[49] We have previously reported that dc-ERG is abnormal in $CFTR$-mutant mice.[25] Our data therefore suggest that the $Myo6^{tvrm89}$ mutation may confer loss of endocytosis of CFTR at the apical RPE and contribute to the reduction in the ERG via altered chloride ion conductances.

Other mouse mutants that demonstrate reduced ERG amplitude in the absence of anatomical changes to the retina include the $Mct3^{-/-}$ mouse, in which the ERG reductions were attributed to altered ion and pH homeostasis in the subretinal space due to the absence of normal lactate transport by monocarboxylate transporter 3 (MCT3).[36] The sodium-driven bicarbonate exchanger (NCBE)–knockout mouse also displays a reduction in b-wave amplitude, with no change in retinal morphology.[37] The altered ERG in this mouse is also thought to result at least partially from impaired intracellular pH regulation and chloride ion concentration. Lysosomal dysfunction can also lead to changes in pH via dysfunction of the ATP-driven proton pump in the RPE membrane.[38]

Loss of $Myo6$ could cause a change in resistance across the retinal circuit through which the ERG is recorded. Such a change could account for an overall reduction in ERG components despite preservation of retinal structure. While it is possible that the adhesions present in the mutant could potentially attenuate the amount of light reaching the retina because of this phenotype, a change in pupil dilation would lead to decreased sensitivity and prolonged latency, which were not observed. Whether any of these potential mechanisms underlie the $Myo6$-mutant phenotype of reduced ERG amplitudes in the face of normal retinal structure will require further analysis.

We have presented a mouse model that can be used to better understand the role of myosin 6 and how it may interact with and compensate for other myosin isoforms. Despite the addition of two small amino acid inserts (amino acids 9 and 13) within the motor domain and a unique 53–amino acid insert between the converter domain and light chain–binding helix, which confers its minus-end directionality,[50] myosin 6 maintains a high degree of homology to other myosin isoforms, most notably in the head-motor domain.[51–54] The phenotypes of $Myo6$-null and $Myo6^{tvrm89}$ mice are similar to that of $Myo7a$

(shaker)–null mice, which is a known Usher IB gene. This mouse mutant also presents with deafness and circling/head tossing behaviors associated with vestibular defects[55,56] and demonstrates reductions in ERG component amplitudes, without photoreceptor degeneration (unless combined with the loss of Cadherin-23, $Cdh23$).[57–61] Most important, Myo7a is also expressed in the RPE and at the actin-rich domain of the inner segment.[62,63] It is interesting to speculate on the potential functional redundancy that may exist between these two myosin isoforms and determine how each acts independently. The generation of mice lacking both $Myo6$ and $Myo7a$ would provide insight into this possibility.

Acknowledgments

References

1. Hartman MA, Finan D, Sivaramakrishnan S, Spudich JA. Principles of unconventional myosin function and targeting. *Ann Rev Cell Dev Biol*. 2011;27:133–155.

2. Wells AL, Lin AW, Chen LQ, et al. Myosin VI is an actin-based motor that moves backwards. *Nature*. 1999;401:505–508.

3. Deol MS, Green MC. Snell's waltzer, a new mutation affecting behaviour and the inner ear in the mouse. *Genet Res*. 1966;8:339–345.

4. Avraham KB, Hasson T, Steel KP, et al. The mouse Snell's waltzer deafness gene encodes an unconventional myosin required for structural integrity of inner ear hair cells. *Nat Genet*. 1995;11:369–375.

5. Hasson T, Mooseker MS. Vertebrate unconventional myosins. *J Biol Chem*. 1996;271:16434.

6. Melchionda S, Ahituv N, Bisceglia L, et al. *MYO6*, the human homologue of the gene responsible for deafness in Snell's waltzer mice, is mutated in autosomal dominant nonsyndromic hearing loss. *Am J Hum Genet*. 2001;69:635–640.

7. Ahmed ZM, Morell RJ, Riazuddin S, et al. Mutations of *MYO6* are associated with recessive deafness, DFNB37. *Am J Hum Genet*. 2003;72:1315–1322.

8. Mohiddin SA, Ahmed ZM, Griffith AJ, et al. Novel association of hypertrophic cardiomyopathy, sensorineural deafness, and a mutation in unconventional myosin VI (*MYO6*). *J Med Genet*. 2004;41:309–314.

9. Sanggaard KM, Kjaer KW, Eiberg H, et al. A novel nonsense mutation in *MYO6* is associated with progressive nonsyndromic hearing loss in a Danish DFNA22 family. *Am J Med Genet A*. 2008;146A:1017–1025.

10. Finsterer J, Fellinger J. Nuclear and mitochondrial genes mutated in nonsyndromic impaired hearing. *Int J Pediatr Otorhinolaryngol*. 2005;69:621–647.

11. Breckler J, Au K, Cheng J, Hasson T, Burnside B. Novel myosin VI isoform is abundantly expressed in retina. *Exp Eye Res*. 2000;70:121–134.

12. Kitamoto J, Libby RT, Gibbs D, Steel KP, Williams DS. Myosin VI is required for normal retinal function. *Exp Eye Res*. 2005; 81:116–120.

13. Lin-Jones J, Sohlberg L, Dose A, Breckler J, Hillman DW, Burnside B. Identification and localization of myosin superfamily members in fish retina and retinal pigmented epithelium. *J Comp Neurol*. 2009;513:209–223.

14. Williams DS, Hallett MA, Arikawa K. Association of myosin with the connecting cilium of rod photoreceptors. *J Cell Sci*. 1992;103(pt 1):183–190.

15. Mochizuki E, Okumura K, Ishikawa M, et al. Phenotypic and expression analysis of a novel spontaneous myosin VI null mutant mouse. *Exp Anim*. 2010;59:57–71.

16. Aschenbrenner L, Naccache SN, Hasson T. Uncoated endocytic vesicles require the unconventional myosin, Myo6, for rapid transport through actin barriers. *Mol Biol Cell*. 2004;15:2253–2263.

17. Aschenbrenner L, Lee T, Hasson T. Myo6 facilitates the translocation of endocytic vesicles from cell peripheries. *Mol Biol Cell*. 2003;14:2728–2743.

18. Park H, Ramamurthy B, Travaglia M, et al. Full-length myosin VI dimerizes and moves processively along actin filaments upon monomer clustering. *Mol Cell*. 2006;21:331–336.

19. Phichith D, Travaglia M, Yang Z, et al. Cargo binding induces dimerization of myosin VI. *Proc Natl Acad Sci U S A*. 2009; 106:17320–17324.

20. Won J, Shi LY, Hicks W, et al. Mouse model resources for vision research [serial online]. *J Ophthalmol*. 2011;2011:391384. Available at: http://www.ncbi.nlm.nih.gov/pmc/articles/ PMC2968714/. Accessed October 11, 2013.

21. Justice MJ, Carpenter DA, Favor J, et al. Effects of ENU dosage on mouse strains. *Mamm Genome*. 2000;11:484–488.

22. Herron BJ, Lu W, Rao C, et al. Efficient generation and mapping of recessive developmental mutations using ENU mutagenesis. *Nat Genet*. 2002;30:185–189.

23. Buffone GJ, Darlington GJ. Isolation of DNA from biological specimens without extraction with phenol. *Clin Chem*. 1985; 31:164–165.

24. Samuels IS, Sturgill GM, Grossman GH, Rayborn ME, Hollyfield JG, Peachey NS. Light-evoked responses of the retinal pigment epithelium: changes accompanying photoreceptor loss in the mouse. *J Neurophysiol*. 2010;104:391–402.

25. Wu J, Marmorstein AD, Peachey NS. Functional abnormalities in the retinal pigment epithelium of CFTR mutant mice. *Exp Eye Res*. 2006;83:424–428.

26. Hasson T, Mooseker MS. Porcine myosin-VI: characterization of a new mammalian unconventional myosin. *J Cell Biol*. 1994; 127:425–440.

27. Brown ME, Bridgman PC. Myosin function in nervous and sensory systems. *J Neurobiol*. 2004;58:118–130.

28. Hertzano R, Shalit E, Rzadzinska AK, et al. A *Myo6* mutation destroys coordination between the myosin heads, revealing new functions of myosin VI in the stereocilia of mammalian inner ear hair cells [serial online]. *PLoS Genet*. 2008;4: e1000207. Available at: http://www.ncbi.nlm.nih.gov/pmc/ articles/PMC2543112/. Accessed October 13, 2013.

29. Self T, Sobe T, Copeland NG, Jenkins NA, Avraham KB, Steel KP. Role of myosin VI in the differentiation of cochlear hair cells. *Dev Biol*. 1999;214:331–341.

30. Hasson T. Unconventional myosins, the basis for deafness in mouse and man. *Am J Hum Genet*. 1997;61:801–805.

31. Hasson T, Mooseker MS. The growing family of myosin motors and their role in neurons and sensory cells. *Curr Opin Neurobiol*. 1997;7:615–623.

32. Shen B, Han X, Jones G, Rossiter SJ, Zhang S. Adaptive evolution of the *Myo6* gene in Old World fruit bats (family: Pteropodidae) [serial online]. *PLoS One*. 2013;8:e62307.

Available at: http://www.ncbi.nlm.nih.gov/pmc/articles/ PMC3631194/. Accessed October 13, 2013.

33. Williams LH, Miller KA, Dahl HH, Manji SS. Characterization of a novel ENU-generated myosin VI mutant mouse strain with congenital deafness and vestibular dysfunction. *Hear Res*. 2013;299:53–62.

34. Chaitin MH, Coelho N. Immunogold localization of myosin in the photoreceptor cilium. *Invest Ophthalmol Vis Sci*. 1992;33: 3103–3108.

35. Mukherjee PK. Examination of iris, ciliary body and choroid. In: *Clinical Examination in Ophthalmology*. New Delhi: Elsevier Health Sciences; 2007:141–157.

36. Daniele LL, Sauer B, Gallagher SM, Pugh EN Jr, Philp NJ. Altered visual function in monocarboxylate transporter 3 (*Slc16a8*) knockout mice. *Am J Physiol Cell Physiol*. 2008; 295:C451–C457.

37. Hilgen G, Huebner AK, Tanimoto N, et al. Lack of the sodium-driven chloride bicarbonate exchanger NCBE impairs visual function in the mouse retina [serial online]. *PLoS One*. 2012;7: e46155. Available at: http://www.ncbi.nlm.nih.gov/pmc/ articles/PMC3467262/. Accessed October 13, 2013.

38. Bergmann M, Schütt F, Holz FG, Kopitz J. Inhibition of the ATP-driven proton pump in RPE lysosomes by the major lipofuscin fluorophore A2-E may contribute to the pathogenesis of age-related macular degeneration. *FASEB J*. 2004;18:562–564.

39. Tumbarello DA, Waxse BJ, Arden SD, Bright NA, Kendrick-Jones J, Buss F. Autophagy receptors link myosin VI to autophagosomes to mediate Tom1-dependent autophagosome maturation and fusion with the lysosome. *Nat Cell Biol*. 2012; 14:1024–1035.

40. Biemesderfer D, Mentone SA, Mooseker M, Hasson T. Expression of myosin VI within the early endocytic pathway in adult and developing proximal tubules. *Am J Physiol Renal Physiol*. 2002;282:F785–F794.

41. Spudich G, Chibalina MV, Au JS, Arden SD, Buss F, Kendrick-Jones J. Myosin VI targeting to clathrin-coated structures and dimerization is mediated by binding to Disabled-2 and PtdIns$(4,5)$P$_2$. *Nat Cell Biol*. 2007;9:176–183.

42. Morris SM, Arden SD, Roberts RC, et al. Myosin VI binds to and localises with Dab2, potentially linking receptor-mediated endocytosis and the actin cytoskeleton. *Traffic*. 2002;3:331–341.

43. Buss F, Arden SD, Lindsay M, Luzio JP, Kendrick-Jones J. Myosin VI isoform localized to clathrin-coated vesicles with a role in clathrin-mediated endocytosis. *EMBO J*. 2001;20:3676–3684.

44. Buss F, Luzio JP, Kendrick-Jones J. Myosin VI: new force in clathrin mediated endocytosis. *FEBS Lett*. 2001;508:295–299.

45. Taylor MJ, Perrais D, Merrifield CJ. A high precision survey of the molecular dynamics of mammalian clathrin-mediated endocytosis [serial online]. *PLoS Biol*. 2011;9:e1000604. http://www.ncbi.nlm.nih.gov/pmc/articles/PMC3062526/. Accessed October 13, 2013.

46. Bond LM, Arden SD, Kendrick-Jones J, Buss F, Sellers JR. Dynamic exchange of myosin VI on endocytic structures. *J Biol Chem*. 2012;287:38637–38646.

47. Collaco A, Jakab R, Hegan P, Mooseker M, Ameen N. α-AP-2 directs myosin VI–dependent endocytosis of cystic fibrosis transmembrane conductance regulator chloride channels in the intestine. *J Biol Chem*. 2010;285:17177–17187.

48. Swiatecka-Urban A, Boyd C, Coutermarsh B, et al. Myosin VI regulates endocytosis of the cystic fibrosis transmembrane conductance regulator. *J Biol Chem*. 2004;279:38025–38031.

49. Ameen N, Apodaca G. Defective CFTR apical endocytosis and enterocyte brush border in myosin VI–deficient mice. *Traffic*. 2007;8:998–1006.

50. Wells A. A cognitive model of generalized anxiety disorder. *Behav Modif*. 1999;23:526–555.

51. Syamaladevi DP, Spudich JA, Sowdhamini R. Structural and functional insights on the myosin superfamily. *Bioinform Biol Insights*. 2012;6:11–21.

52. Ahituv N, Sobe T, Robertson NG, Morton CC, Taggart RT, Avraham KB. Genomic structure of the human unconventional myosin VI gene. *Gene*. 2000;261:269–275.

53. Vibert P, Cohen C. Domains, motions and regulation in the myosin head. *J Muscle Res Cell Motil*. 1988;9:296–305.

54. Warrick HM, Spudich JA. Myosin structure and function in cell motility. *Ann Rev Cell Biol*. 1987;3:379–421.

55. Gibson F, Walsh J, Mburu P, et al. A type VII myosin encoded by the mouse deafness gene shaker-1. *Nature*. 1995;374:62-64.

56. Weil D, Blanchard S, Kaplan J, et al. Defective myosin VIIA gene responsible for Usher syndrome type 1B. *Nature*. 1995; 374:60–61.

57. Libby RT, Kitamoto J, Holme RH, Williams DS, Steel KP. *Cdh23* mutations in the mouse are associated with retinal dysfunction but not retinal degeneration. *Exp Eye Res*. 2003;77:731–739.

58. Libby RT, Steel KP. Electroretinographic anomalies in mice with mutations in *Myo7a*, the gene involved in human Usher syndrome type 1B. *Invest Ophthalmol Vis Sci*. 2001;42:770–778.

59. Lillo C, Kitamoto J, Liu X, Quint E, Steel KP, Williams DS. Mouse models for Usher syndrome 1B. *Adv Exp Med Biol*. 2003;533:143–150.

60. Keats BJ, Corey DP. The Usher syndromes. *Am J Med Genet*. 1999;89:158–166.

61. Jacobson SG, Cideciyan AV, Gibbs D, et al. Retinal disease course in Usher syndrome 1B due to *MYO7A* mutations. *Invest Ophthalmol Vis Sci*. 2011;52:7924–7936.

62. Gibbs D, Diemer T, Khanobdee K, Hu J, Bok D, Williams DS. Function of MYO7A in the human RPE and the validity of shaker1 mice as a model for Usher syndrome 1B. *Invest Ophthalmol Vis Sci*. 2010;51:1130–1135.

63. Williams DS, Lopes VS. The many different cellular functions of MYO7A in the retina. *Biochem Soc Trans*. 2011;39:1207–1210.